Assessment of stress shielding around a dental implant for variation of implant stiffness and parafunctional loading using finite element analysis

MUHAMMAD IKMAN ISHAK[1]*, RUSLIZAM DAUD[1], SITI NOOR FAZLIAH MOHD NOOR[2],
C.Y. KHOR[1], HUSNIYATI ROSLAN[2]

[1] Fakulti Kejuruteraan & Teknologi Mekanikal, Universiti Malaysia Perlis (UniMAP),
Kampus Alam UniMAP, Pauh Putra, 02600 Arau, Perlis, Malaysia.
[2] Advanced Medical and Dental Institute, Universiti Sains Malaysia, Bertam,
Jln. Tun Hamdan Sheikh Tahir, 13200 Kepala Batas, Pulau Pinang, Malaysia.

Purpose: The aim of this study was to evaluate the mechanical stimuli transfer at the bone-implant interface via stress and strain energy density transfer parameters. This study also aimed to investigate the effect of different implant stiffness and parafunctional loading values on the defined mechanical stimuli transfer from the implant to the surrounding bone. *Methods*: A three-dimensional finite element model of two-piece threaded dental implant with internal hexagonal connection and mandibular bone block was constructed. Response surface method through face-centred central composite design was applied to examine the influence of two independent factors variables using three levels. The analysis model was fitted to a second-order polynomial equation to determine the response values. *Results*: The results showed that the implant stiffness was more effective than the horizontal load value in increasing the stress and strain energy density transfers. The interaction between both factors was significant in decreasing the likelihood of bone resorption. Decreasing the implant stiffness and horizontal load value led to the increased stress transfer and unexpected decrease in the strain energy density, except at the minimum level of the horizontal load. The increase in the implant stiffness and horizontal load value (up to medium level) have increased the strain energy transfer to the bone. *Conclusions*: The stress and strain energy density were transferred distinctively at the bone–implant interface. The role of both implant stiffness and parafunctional loading is important and should be highlighted in the pre-operative treatment planning and design of dental implant.

Key words: dental implant, finite element analysis, implant stiffness, parafunctional loading, stress shielding

1. Introduction

Stress shielding is a well-known phenomenon in biomechanics, describing the effect of different elastic modulus of metallic implant and its surrounding bone tissue [29]. In this situation, the implant prevents the bone from acquiring a necessary stress or strain level, which is beneficial for bone remodelling process. The intensity of bone stress or strain produced is highly dependent on how well the mechanical stimuli is being transferred from the implant. Low stress or strain stimulus can attribute the bone to the decreased mass and strength, resulting in unfavourable bone resorption. This leads to the implant loosening and fracture. Evidence of bone loss in the vicinity of implants has been reported in clinical radiologic assessments [7], [34]. In contrast, high stress or strain stimulus can cause the bone to increase its mass and corresponding strength. Earlier findings suggested that a constant compression at the bone-implant interface or mechanical stimuli transmitted to the bone should be attained for normal

bone remodelling [9], [28]. At present, high attention of stress shielding effect is given to the field of long bone studies [29], little is known of that in the field of implant dentistry.

With regard to material stiffness of dental implant, the range of elastic modulus for regular metallic implants used in tooth restoration is from 104 100 to 117 000 MPa, for pure titanium and its alloy. The jawbone tissues surrounding the implant body, on the contrary, possess a much lower elastic moduli which are in the range of 1500–46 100 MPa and 3.5–950 MPa for the cortical and cancellous bone, respectively [25]. The unequal shared load at the bone–implant interface after physiological loading has caused the softer structure (bones) to be atrophied. Ceramics, such as zirconia, are also the common option of implant materials with additional advantage of fulfilling aesthetic demand from the patients. Besides, zirconia alloy with titanium or titanium zirconium (TiZr) is also introduced to improve the properties of pure materials as TiZr offers better tensile strength, biocompatibility, hardness and corrosion resistance [6]. Dental implants made of polymers or polymeric reinforced composites (polyetheretherketone (PEEK)) have stiffness (3–4 GPa) comparable with that of the bone and relatively lower than other implant materials [21]. The PEEK promotes good mechanical, thermal and chemical abrasion resistances, not to mention, resistance to hydrolysis, and great biocompatibility. Currently, the effect of different materials on the implant performance remains a subject of debate and uncertainty.

Apart from material stiffness that could influence the response of implant and adjacent bone, parafunctional oral habits also play a vital role. Clenching, bruxism and ice chewing are the examples of parafunctional oral habits attributing the patients to sustain a greater cyclic occlusal force [3] which is likely to yield implant fatigue failure [33]. The value of loading could even be higher by tongue thrust due to tongue perioral forces and circumoral musculature [4]. Bruxism, in particular, is one of the contributing factors in the technical failure of dental implant. When the occlusal force is exerted on the implant, it is resolved into vertical and horizontal force parts. The vertical force acts along the longitudinal axis of the implant, while the horizontal force acts along the bucco-lingual and mesio-distal axes. The value of horizontal force is relatively lower (up to one-tenth of the vertical force), however, it could leave significant adverse impact on the implant stability. Some studies reported no association between bruxism and implant failure [18], thus further analysis is necessary.

The reaction of implant-bone complex towards loading is associated with Wolf's law that indicates that every change in the form and function of a bone is followed by certain definite changes in their internal architecture and equally definite secondary alterations in their external conformation, in accordance with mathematical laws [19]. Thus, biomechanical behaviour of an implanted fixture may be described by the stress (or other mechanical stimuli) dissemination within the surrounding bone. Concerning the type of mechanical stimuli that can be accountable in triggering the bone remodelling process, majority researchers prefer strain energy density to be used [9]. It is a necessity to quantify how altered implant stiffness and parafunctional loading value reflect upon mechanical stimuli distributions in the bone. Computational simulation methods such as finite element analysis (FEA) are popular and useful for examining the biomechanical characteristics in the analytic model of artificial tooth [30], [40]. This method can help investigators determine the result parameters which are difficult to be obtained in *in vitro* and *in vivo* works. Apart from structural mechanics, FEA is also used to solve problems in other related fields or aspects such as thermal, fluid [14], [23], fracture and fatigue [1]. Many previous computational analyses have been performed on dental implant [10], [11], [13], [26], however, low emphasis is placed on the parameters associated to stress shielding effects.

The main goal of this study was to evaluate whether significant differences observed between the stress and strain energy density distributions at the bone-implant interface under implant loading. Here, a three-dimensional (3-D) FEA was used to simulate the exertion of compressive dynamic loading on endosseous dental implant that was inserted into the bone. Two types of criteria that have previously been defined, which are stress transfer parameter (STP) and strain energy density transfer parameter (SEDTP), were considered for the interpretation of results. These parameters enabled us to compare the mechanical stimuli transfers to the surrounding bone based on the alterations in implant stiffness and parafunctional loading values. Comparing the findings could shed light on which implant stiffness and parafunctional loading values resulting in higher mechanical stimuli transfer to the adjacent bone. Furthermore, by applying response surface method (RSM) to fit statistical model through experimental design like face-centered central composite design (CCD), the effect of independent input factors (implant stiffness and parafunctional loading) and their interactions on response variables can be described.

2. Materials and methods

2.1. Analytical models generation

A 3D model of prosthetic treatment through a single restoration was manifested by a defect in the left mandibular first molar. The bone area covering the second premolar and second molar was also prepared as the region of interest. In this study, the analytic model comprised a number of parts which are: cortical bone, cancellous bone, implant body, abutment, abutment screw, metal framework and prosthesis (crown). An implant of Alpha-Bio Tec, Petach Tikva, from dual-fit type (DFI) with internal hexagonal connection and trapezoidal-shaped thread was used and placed at the first molar site. The implant body was designed to be 11.5 and 3.75 mm for the length and diameter, respectively, using a computer-aided design software, SolidWorks 2020 (SolidWorks Corp., Concord, Massachusetts, USA). The abutment (height: 3.5 mm) and abutment screw (length: 8.0 mm; width: 2.2 mm) were also created using the same software through in-built geometry features such as sweep, extrude, loft, and/or revolve. The screw is employed to hold the abutment body in place which attached to the implant body. Meanwhile, for the 3D hard tissue models (cortical and cancellous bones), they were developed by processing a series of computed tomography (CT) image dataset of a skull with an image-processing software, Mimics 20.0 (Materialise, Leuven, Belgium). The cortical and cancellous bones were distinguished between one another by thresholding the images based on density scale. The mandibular canal located at the inferior side was neglected in the modelling. To assure the accuracy of bone anatomical structures, the developed bone block model was qualitatively compared to the virtual mandibular bone from 3D human anatomy software, Complete Anatomy (3D4Medical, Elsevier). For simplification, the mesial, distal, inferior and superior parts of the bone block were flattened to produce well oriented meshing elements. As a result, the bone segment with dimensions of 30 mm (length) × 20 mm (high) × 8 − 10 mm (width) was created. The cortical layer was 2-mm thick, and the whole internal volume was considered to be solid cancellous bone. These dimensions are also comparable with those provided in several previous numerical studies that researched similar bone region [32], [41]. The CT model of the first molar was altered to construct a full prosthesis or crown. This was done by keeping only the coronal portion of the tooth, whilst the root was removed. A simplified geometrical shape of metal framework was also designed by reducing the size of prosthesis model by about 30%.

All the models described above were then imported into SolidWorks software to generate solid geometries before establishing virtual surgery simulation. The implant was positioned orthogonally to the
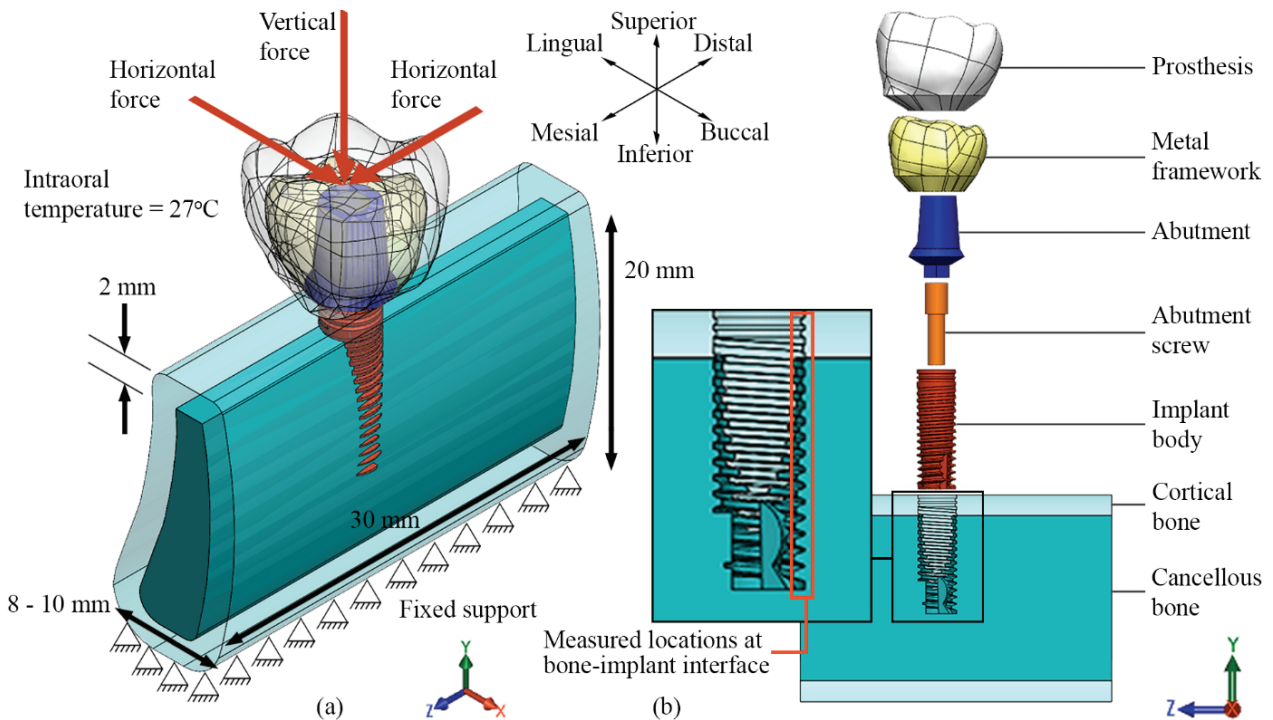

Fig. 1. (a) Assembled analytic model showing the fixed support and masticatory forces, (b) Exploded view of the analytic model

occlusal plane. The longitudinal axes of the abutment, abutment screw, and implant body were aligned. The flat surface of implant platform was set to correspond with the top plane of the cortical bone mimicking clinical bone-level implant placement. A 3.75-mm wide cylindrical hole was prepared in the middle of the bone model to represent implant bed using "combine" and "subtract" tools. The prepared bone model was then exported into ANSYS software (ANSYS Inc., Houston, TX, USA) with the completed implant system being inserted prior to the analysis. The assembled and exploded configurations of analytic models employed in the study are depicted in Fig. 1.

2.2. Finite element modelling

A perfectly bonded connection (continuous displacement) was assigned at the contact surfaces between the implant body and bone, simulating bone-to-implant interface completion (100% osseointegration). Similar contact condition was assumed at the interfaces of the cortical and cancellous bones. Non-linear frictional contact condition with the friction coefficient, μ value of 0.3 [37] was applied to simulate the attachment of the implant body/abutment screw, abutment/abutment screw, abutment/metal framework and prosthesis/metal framework. The contact surfaces were adopted with Augmented Lagrange method and the contact detections were based on Gauss integration point.

Table 1. Mechanical properties of materials used based on the literatures

Material	Elastic Modulus, E [GPa]	Poisson's Ratio, v	Shear Modulus, G [GPa]	Reference
Cortical bone	$E_x = 17.9$ $E_y = 12.5$ $E_z = 26.6$	$v_{yz} = 0.31$ $v_{xy} = 0.26$ $v_{xz} = 0.28$	$G_{yz} = 5.3$ $G_{xy} = 4.5$ $G_{xz} = 7.1$	[31]
Cancellous bone	$E_x = 1.148$ $E_y = 0.021$ $E_z = 1.148$	$v_{yz} = 0.055$ $v_{xy} = 0.003$ $v_{xz} = 0.322$	$G_{yz} = 0.068$ $G_{xy} = 0.068$ $G_{xz} = 7.1$	[31]
Ti-6Al-4V	113.8	0.342	–	[41]
Feldspathic porcelain	82.8	0.35	–	[36]
CoCr alloy	218	0.33	–	[6]

The properties of materials used for all structures are exhibited in Table 1. In this study, the cortical and cancellous bones were considered as anisotropic and linearly elastic materials, whereas the implant and prosthesis components were assumed to be isotropic, linearly elas-

tic, and homogenous. The prosthesis, metal framework, and abutment and screw were made of feldspathic porcelain, cobalt-chromium (CoCr) alloy and Ti-6Al-4V, respectively. The anisotropic materials show different mechanical properties based on loading direction. For the mandibular bone, the elastic modulus is the highest along the mesio-distal direction (0°, longitudinal), and the lowest along the corono-apical or bucco-lingual direction (90°, transverse). On the other hand, the isotropic materials exhibit similar mechanical properties irrespective of loading direction. Three different values of material stiffness for the implant body analysed with the basic (average) value set in the study was 109 000 MPa.

The finite element analyses were composed of two main loading types which are human masticatory load and screw pretension. A variation of 300 N [41] dynamic masticatory load represented chewing action being simulated in a manner that interpreted different vertical (y-axis) and horizontal (x- and z-axis) force components. The variation was made based on three different load angulations (0°, 30° and 90°). These angles were set buccolingually to the central axis of the implant. The horizontal and vertical force components resolved from the 300 N load at each load inclination are shown in Table 2. The increased horizontal load or the decreased vertical load value indicates the increased inclination of occlusal force from 0° to 90°. The loading inclination signifies the increase in the intensity of parafunctional loading. The basic (average) value of the horizontal and vertical force components was 106.07 N and 259.8 N, respectively, which was determined at the load angulation of 30°. The loads were applied onto the top surface of the prosthesis (Fig. 1a). A screw pretension of 20 N [41] corresponds to tightening torque that was imposed on the abutment screw. The temperature of intraoral or environment was set to 27°C constantly. For the model supports, the bottom surface of the bone block was taken as fixed constraint, therefore, other surfaces were free of the condition [41]. The fixed constraint was applied at all degrees of freedom of the nodes of the stated surface.

Table 2. Vertical and horizontal force components at three different load inclinations

Load Inclination	Horizontal Force Component (x- and z-axes)	Vertical Force Component (y-axis)
0°	0 N	300 N
30°	106.07 N	259.8 N
90°	212.13 N	0 N

It is noteworthy that the results of FEA should be free from all numerical factors. Also, the results of FEA only provide an approximate solution to the problem. Therefore, a mesh convergence test was performed to ensure that the findings were independent from mesh configuration. The analytic models were meshed with solid linear tetrahedral elements of four nodes using meshing tools in ANSYS software. The sensitivity of the mesh was defined by measuring the maximum principal stress value in the bone, STP Total, and SEDTP Total for different mesh density sets. Six mesh density sets were prepared: Tet-A – 190 000 elements, Tet-B – 260 000 elements, Tet-C – 410 000 elements, Tet-D – 750 000 elements, Tet-E – 1 083 000 elements, and Tet-F – 1 690 000 elements. The final element number is adopted when the variation of the result is less than 5%. The outcome of the test showed that there was inconsiderable difference of the maximum principal stress magnitudes recorded among the model sets. Meanwhile, for the mechanical stimuli transfer results, the STP and SEDTP Total exhibited the deviation percentage of 3.6% and 5.0%, respectively, after two refinements. Overall, the results appeared to yield at the number of elements and nodes of about 410 000 and 613 000, respectively. Therefore, the mesh configuration of Tet-C was chosen for the analysis models. A plot of maximum principal stress, STP Total, SEDTP Total and mesh distribution in the model before (Tet-A) and after two refinements (Tet-C) are illustrated in Fig. 2. For verification purpose, the proposed model through the chosen mesh density was then compared with past investigations that evaluating similar prosthetic treatment and implant location. The analysis input settings in those works were duplicated, excluding the model geometry. Equivalent von Mises stress in the bone was extracted for the comparison. It was exhibited that the maximum bone stress in our model was comparable with the one recorded in previous studies, as shown in Table 3.
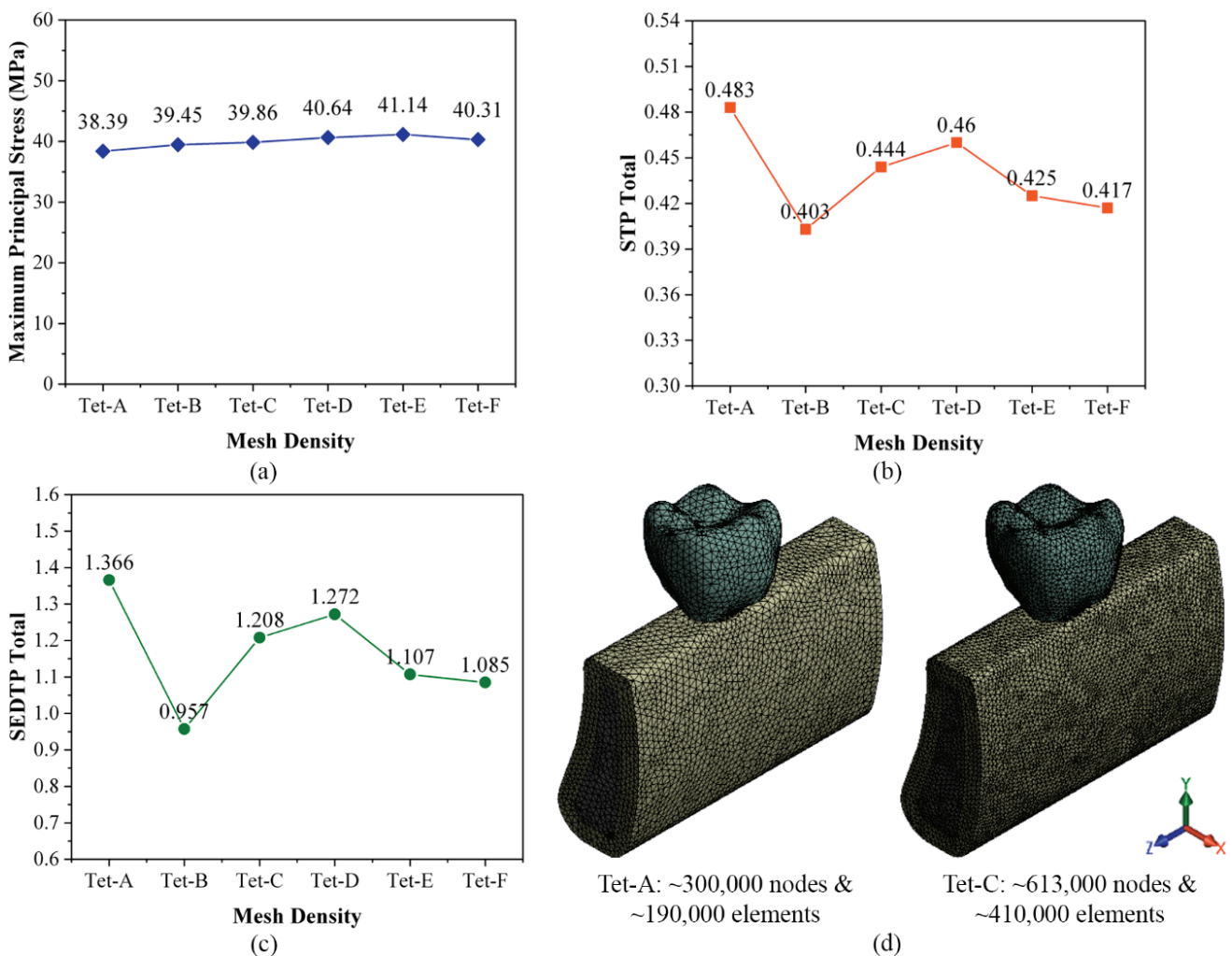

Fig. 2. (a) Maximum principal stress, (b) STP Total, (c) SEDTP Total values for different mesh densities,
(d) comparison of mesh plot in the model before (Tet-A) and after two refinements (Tet-C)

Table 3. Comparison of bone equivalent von Mises stress
between literature and our model

Previous Study	Literature Results	Proposed Model Results
[32]	Bone: 17.00 MPa	Bone: 19.13 MPa
[41]	Bone: 20.93 MPa	Bone: 29.93 MPa

2.3. Design of experiments (DOE)

In the present study, a total of 9 analysis runs have been determined from face-centered CCD via RSM, based on two independent biomechanical design factors – implant stiffness and parafunctional loading. The response variables were the stress shielding data which are STP and SEDTP. The STP is computed using the following equations [8], [9],

$$\text{STP}\alpha = \frac{\sigma_b}{\sigma_t}, \quad (1)$$

$$\text{STP}\beta = \sum_{i=j=2}^{i=j=N} \frac{\sigma_{bi}}{\sigma_{tj}}, \quad (2)$$

$$\text{STP Total} = \text{STP}\alpha + \text{STP}\beta, \quad (3)$$

and the SEDTP can be expressed as [9]

$$\text{SEDTP}\alpha = \frac{\sigma_b \varepsilon_b}{\sigma_t \varepsilon_t}, \quad (4)$$

$$\text{SEDTP}\beta = \sum_{i=j=2}^{i=j=N} \frac{\sigma_{bi} \varepsilon_{bi}}{\sigma_{tj} \varepsilon_{tj}}, \quad (5)$$

$$\text{SEDTP Total} = \text{SEDTP}\alpha + \text{SEDTP}\beta. \quad (6)$$

The STP α and STP β are the ratios of average equivalent von Mises stress to the bone, σ_b and average equivalent von Mises stress to the implant thread, σ_t. Whilst, the SEDTP α and SEDTP β are the ratios of average stress-strain relation where σ is equivalent von Mises stress and ε is equivalent von Mises strain. Subscripts b and t represent bone and implant thread, respectively. Subscript i indicates the bone volume located between the threads excluding the first thread, and subscript j indicates the threads of the implant excluding the first thread.

17 points at the bone–implant interface (Fig. 1b) were analysed on a two-dimensional plane along the mesio-distal axis to extract the equivalent von Mises stress and strain prior to the calculation of STP and SEDTP. The stress and strain maps were also plotted for qualitative analysis. The design space is defined at three different levels of –1, 0, and 1 for each factor. The sets of independent input variables for each run are shown in Table 4. It is important to note that only horizontal load component was considered in DOE to represent the variation of parafunctional loading. However, the corresponding vertical load component at each load inclination was still simulated as indicated in Table 2 in the analyses. The reason behind this was to ensure that the coupling of the horizontal and vertical force components could be achieved in accordance with the force resolution determined. All response data were analysed using a statistical analysis through the least square method in polynomial regression model. A second order of polynomial equation is fitted to the numerical data, which can be expressed in Eq. (7), where Y is the response variable, X_i and X_j are the input variables, β_0 is the constant coefficient, β_i, β_{ii}, and β_{ij} are the coefficient of linear, quadratic and interaction terms, respectively, k is the number of input variable and ε is the error.

$$Y = \beta_0 + \sum_{i=1}^{k} \beta_i X_i + \sum_{i=1}^{k} \beta_{ii} X_i^2 + \sum_{i=1}^{k} \sum_{i \neq j=1}^{k} \beta_{ij} X_i X_j + \varepsilon. \quad (7)$$

Table 4. Numerical experimental layout

Analysis Run	Implant Stiffness [MPa]	Horizontal Load Component [N]
1	200 000	106.07
2	109 000	106.07
3	18 000	212.13
4	109 000	0
5	109 000	212.13
6	18 000	106.07
7	200 000	0
8	200 000	212.13
9	18 000	0

3. Results

3.1. STP and SEDTP results

The calculated response variables for each analysis run are depicted in Table 5. Our findings showed that the highest STP Total was generated in analysis run 9 with a magnitude of 1.626, and the minimum one was recorded in analysis run 7 with a magnitude of 0.334. The maximum and minimum values of STP Total were generated by the combination of implant stiffness = 18 000 MPa and horizontal load = 0 N, and implant stiffness = 200 000 MPa and horizontal load = 0 N, respectively. In general, it was revealed that

Table 5. Results of numerical experiments

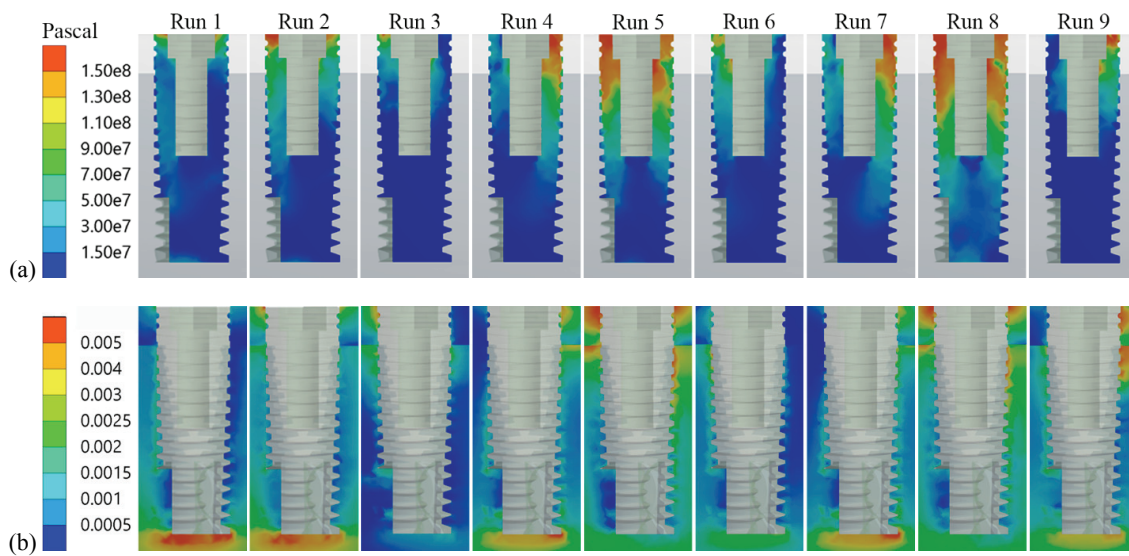| Run	STP α	STP β	STP Total	SEDTP α	SEDTP β	SEDTP Total
1	0.624	0.161	0.786	4.135	1.204	5.339
2	0.700	0.182	0.882	3.109	0.983	4.091
3	0.927	0.379	1.306	0.969	0.740	1.710
4	0.403	0.133	0.535	0.995	0.466	1.462
5	0.451	0.109	0.561	1.321	0.449	1.770
6	1.203	0.272	1.474	1.454	0.670	2.124
7	0.255	0.078	0.334	0.740	0.326	1.066
8	0.385	0.071	0.456	1.584	0.365	1.949
9	1.034	0.592	1.626	1.212	1.569	2.781

Fig. 3. (a) Contour plots of equivalent von Mises stress in the implant body,
(b) contour plots of equivalent von Mises strain in the adjacent bone

a decrease in material stiffness resulted in a rise in STP Total rather than the influence of horizontal load. Nonetheless, contradictory outcomes were discovered for SEDTP Total, where high implant stiffness recorded the greatest (5.339) and least (1.066) values. In this scenario, the horizontal load had a greater impact than the implant stiffness evidenced by the maximum and minimum SEDTP Total values were recorded by the combination of factors of implant stiffness = 200 000 MPa and horizontal load = 106.07 N (analysis run 1), and implant stiffness = 200 000 MPa and horizontal load = 0 N (analysis run 7), respectively. Higher STP and SEDTP Total values indicate a greater potential of stress and strain energy density being transmitted at the bone–implant contact, respectively. As it dictates the mechanical stresses to be shielded in avoiding peri-implant bone loss, the results are predicted to be at their peak.

The stresses were widely distributed in the corono-apical direction and were substantially localized at the implant neck, as shown in Fig. 3a. When the implant stiffness was lowered, there was less stress dispersion and the formation of a less concentrated zone (i.e., analysis runs 3, 6, and 9). As shown in Fig. 3b, an implant with a smaller horizontal load appeared to tolerate a larger amount of von Mises strain, resulting in a more substantial strain rise and distribution to the neighbouring bones (i.e., analysis runs 4, 7, and 9). The elevated strains were intensified mostly at the implant neck and tip.

3.2. Statistical analysis

The responses of the models due to the variation of implant stiffness and parafunctional loading were statistically analysed further using ANOVA. The regression coefficients of linear, quadratic and interaction in the model were examined. In addition, all terms were validated using 95% confidence interval probability values. The model's effectiveness was assessed through the *F*-value and the modified coefficient of determi-

nation (R_{adj}^2). The *F*-values of the model for STP and SEDTP Total were 36.41 and 9.25, respectively. Meanwhile, for the R_{adj}^2, STP Total recorded a value of 93.65% which was higher than that of SEDTP Total which was merely 67.43%. Mathematical models were developed by fitting the second-order polynomial equation to the response data. The final mathematical models constructed in terms of real factors are presented in Eqs. (8) and (9), where *A* represents implant stiffness and *B* represents horizontal load.

$$STP\ Total = 1.76934 - (1.5 \times 10^{-1} \times A) +$$
$$(0.003556 \times B) + (1.14485 \times 10^{-8} \times A \times B) +$$
$$(3.7789 \times 10^{-11} \times A^2) - (2.4 \times 10^{-5} \times B^2), \quad (8)$$

$$SEDTP\ Total = 1.9614 - (5.98638 \times 10^{-7} \times A) +$$
$$(0.035697 \times B) + (5.06117 \times 10^{-8} \times A \times B) +$$
$$(7.2684 \times 10^{-12} \times A^2) - (0.000193 \times 10^{-5} \times B^2). \quad (9)$$

3.3. Main effect and interaction of factors

The perturbation plots of the factors towards response data to describe the deviation of each factor from reference point are illustrated in Fig. 4. The reference point of the plots was set at the basic level of material stiffness and horizontal load component which are 109 000 MPa and 106.07 N, respectively. Optimum value of STP and SEDTP Total only ex-

isted for the horizontal load factor, compared to the implant stiffness factor. However, both implant stiffness and horizontal load component factors have substantial impact on the stress shielding parameters. The STP Total was found to be at the intermediate value for the implant stiffness, while maximum – for the horizontal load at the basic level. A similar discovery was made for the SEDTP Total results. As implant stiffness increases, STP Total at the bone–implant contact decreases. The decremental gradient of the result, however, is minimal in high implant stiffness. For the SEDTP Total, a reversal was seen along with an increase in implant stiffness resulting in an increase in SEDTP data, with a negligible difference in increment at basic and high input variable levels. The inverse trend was depicted for the horizontal load component. The SEDTP Total findings are heavily influenced by the horizontal load value, whereas the STP Total is heavily influenced by the implant stiffness. This might be explained by a steeper curvature shown, designating a significant change in responses.

The interaction plot could visualise the relationship between both input independent factors. This plot may also allow us to know when the interaction of two input variables affects the responses. As illustrated in Fig. 5, the implant stiffness and horizontal load component are highly related to one another as shown by the intersection of plotted data. In low implant stiffness, increasing the horizontal load value is less efficient in increasing the STP Total. Nevertheless, for the implant with high stiffness, the increase in the horizontal load has considerably increased the
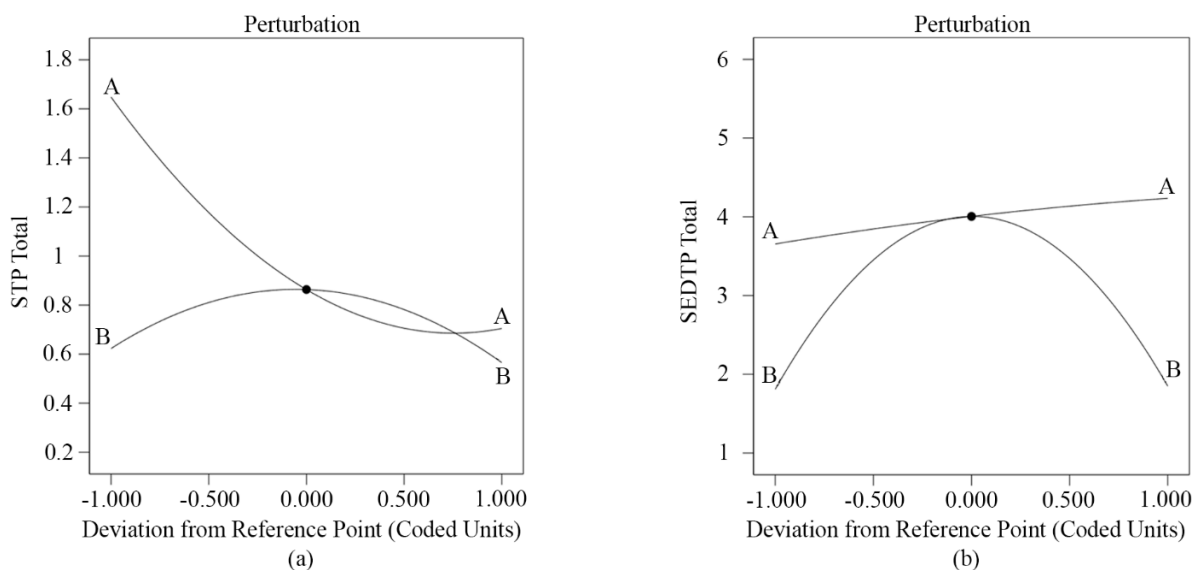

Fig. 4. Perturbation plot for (a) STP and (b) SEDTP Total.
A and B representing implant stiffness and horizontal load component, respectively
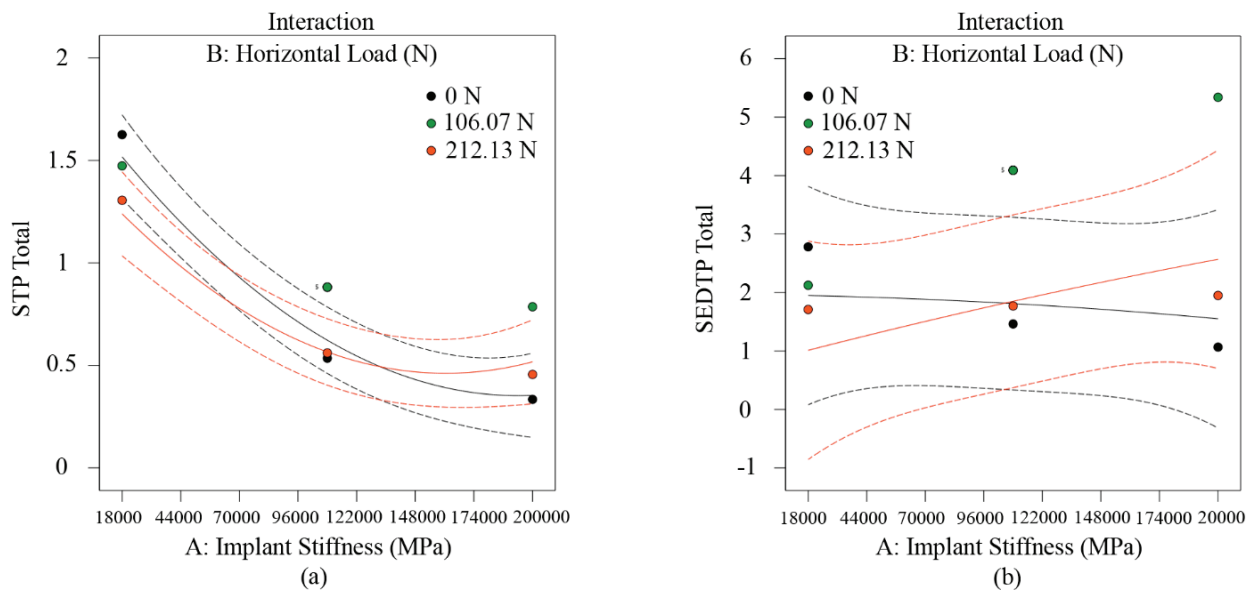
Fig. 5. Interaction plot for (a) STP and (b) SEDTP Total

value of STP Total. Similar interaction pattern was observed for the SEDTP Total result data.

4. Discussion

This study evaluated the effect of different implant stiffnesses and parafunctional loading conditions on stress shielding in order to quantify the transfer of mechanical stimuli between the implant and adjacent bone. Mechanical stimuli are important in providing regular bone maintenance [35]. A larger transmission of mechanical stimuli from a metallic implant to the neighbouring bones may decrease the impact of detrimental stress shielding. The actual mechanical stimuli that triggering bone remodelling are still unknown, however, majority theorists have proposed stress [38] and strain energy density [39] as the reliable candidates.

By simulating the influence of two main biomechanical design factors, we were able to observe the value and distribution of STP and SEDTP in our bone-implant assembly. In general, the dispersion of mechanical stresses within the implant body was consistent with the predicted patterns reported in other finite element studies [16], [24]. The force was longitudinally distributed along the length of the implant body and highly concentrated at the implant neck, regardless of the analysis runs investigated. Stress has also been found to be the greatest at the region surrounding the first few threads, exposing the threads to high shear.

Stress shielding implications are more significant when stiffer implants are adopted. Considering this

reason, we varied the value of elastic modulus of the implant body from 18 000 MPa (low stiffness), followed by 109 000 MPa (medium stiffness), and 200 000 MPa (high stiffness), expecting a decrease in mechanical stimuli transfer to the bone. As predicted, the reduced implant elastic modulus led to the increased value of stress (STP) transmitted. This is parallel with the findings of previous numerical works [2], [32]. One study by Bataineh and Al Janaideh [2] reported that implant made of carbon fibre-reinforced PEEK (E: 18 000 MPa) demonstrated a higher bone stress compared to Ti-6Al-4V implant (E: 110 000 MPa). This is consistent with those of Schwitalla et al. [32], who claimed that the marginal bone stress level was amplified by PEEK implants. Surprisingly, the strain energy density (SEDTP) was counter-intuitive in respect to the decreasing elastic modulus. This is evidenced by a lower value of SEDTP recorded for a reduced modulus of elasticity. A possible explanation is that for the less stiff implant, high restriction could be imposed on the implant structure that resulting in the low implant strain produced. The stiffer implant, on the contrary, possesses a lower resistance which attributed the implant to have higher strain. However, further analyses in the perspective of bone-implant interaction are demanded to clearly scrutinise the situation.

Patients with parafunctional oral habit have been shown to produce different stress and strain levels relative to those with normal masticatory behaviour. In this present study, we varied the parafunctional loading by value in terms of vertical and horizontal force components, in order to assess the resulting

stress and strain energy density. The horizontal forces (0, 106.07, and 212.13 N) were highly emphasised in this study as it could leave more adverse effect on the implant. In masticatory movement, it is impossible to avoid the presence of lateral force although the lateral movements of the mandible are restricted. Our results demonstrated that an increase in the magnitude of horizontal load exhibited an increase in both STP and SEDTP data. However, for the SEDTP, the increase was up to medium level only. The findings agreed with the FEA results by Kim et al. [15], where the 100-N axial load (without the horizontal force component) generated a lower stress value (257.16 and 304.65 MPa) in the implant compared to the similar load at 15° angulation (677.28 and 687.80 MPa) for a variation of implant designs. Marcián et al. [20] drew similar conclusion that the lateral forces leave undesirable bone strains and implant body stresses under their investigation on the influence of different loading conditions. Besides, another study also showed consistent findings in which 150-N oblique load at 45° inclination a greater cortical (150 MPa) and cancellous bone (15 MPa) stresses than the pure vertical load (cortical: 73 MPa, cancellous: 6 MPa) [17].

Mechanical stimuli transfer indicated by the increased value of STP and SEDTP for the implant stiffness was greater in comparison to the horizontal load value. Besides, the deviation of the SEDTP results was more pronounced by the change of the horizontal load magnitude compared to that of the implant stiffness. This finding corresponds with the value of R^2_{adj} for SEDTP which was lower (67.43%) than the one for STP data (93.65%), indicating that less variability of SEDTP data towards the change of factor variables, particularly the horizontal load value. It is, therefore, suggested here that the strain energy density at the bone-dental implant interface should be evaluated more closely in future investigations.

As far as stress at the bone–implant interface was concerned, the maximum level of bone equivalent von Mises stress generated in all analysis runs was substantially lower than the strength of the cortical bone, 170 MPa. Our results depicted that the greatest bone stress value at the bone-implant interface was 93.25 MPa (~1.8-fold lower) recorded in analysis run 9, while the lowest was 2.18 MPa (~78 times lower) recorded in analysis run 6. All the bone stress magnitudes were consistent with those published in the earlier studies that consider similar region of interest and prosthetic treatment [27], [31], [32]. Meanwhile, for the implant stress, all maximum values recorded were also below than the yield strength (YS) of each corresponding material defined. For the very soft material (i.e., poly-

mer) represented by $E = 18\,000$ MPa, the peak stress in the implant was merely 90.19 MPa, which was considerably lower than the YS of polymeric implant material such as PEEK, 260 MPa. Regular stiff material (i.e., Ti-6Al-4V) designed by $E = 109\,000$ MPa, the highest implant stress was 126.42 MPa, which was about ~7-fold lower than the YS of the material (880 MPa). Mimicking a very hard material (i.e., zirconia) through $E = 200\,000$ MPa, the maximum implant stress level recorded was 148.16 MPa, which was also lower than the YS of the material (2000 MPa). For the equivalent von Mises strain results, we evaluated the data based on Frost's mechanostat theory [5]. It is described that the strain level that is higher than 2500 μ could attribute the bone to physiologic overload due to microscopic fatigue damage. Pathologic overload, on the other hand, is predicted if the strain exceeds 4500 μ. From the analyses, only one strain data (3135.2 μ – analysis run 7) showed the likelihood of physiologic overload occurrence and two strain results (5060.8 μ – analysis run 8, and 6906.8 μ – analysis run 9) expecting pathologic overload. Our findings seemed to correlate with those of a past study where unfavourable strain level was reported in the bone predicting pathological bone disruption [2]. Considering these unexpected results which do not correspond well with clinical observations, one may propose different strain threshold category uniquely for the justifications of the alveolar bone strain distribution in dental implantology. Peri-implant or marginal bone loss plays a vital influence on the perseverance of an endosseous dental implant, and it is one of the main manifestations in implant dentistry regarding osseoinsufficiency [12]. The bone resorption may result in many adverse implications, namely, poor prosthetic outcome, tissues deformation, patient dissatisfactions and implant extraction [22]. It was reported that the decrease in the bone height was more pronounced in the first year of treatment, which is about 1.0 mm. The bone level decrease, nevertheless, was reduced to only 0.2 mm for the subsequent years. Critical loosening and severe fracture of the implant owing to the loss of surrounding bone volume could lead to eventual implant removal. Thus, the unfavourable effects of the marginal bone resorption must be reduced by attaining optimum bone-implant interaction.

From the RSM results (interaction analysis) obtained, we found that the implant stiffness and horizontal load value appeared to be greatly correlated to one another. In that respect, the role of both factors should be addressed in the pre-operative treatment planning and design of dental implant. High mechanical stimulus (STP) was noticed when the less stiff

implant and low value of horizontal load were used. The level of STP was decreased if the stiffer implant and low value of horizontal load was employed. However, it is noteworthy that the increase in the horizontal load magnitude is more influential in increasing the STP for the high stiff implant. Therefore, the perseverance of high stiff implant for patients with severe parafunctional oral habits may be improved by adopting more flexible implant to avoid the unwanted stress shielding effects. Another mechanical stimulus, SEDTP, presented a contradictory outcome relative to STP, as explained earlier, which is also in agreement with a computational study of orthopaedic screw-bone construct by Haase and Rouhi [9] and this requires more attention in future works.

Simulating clinical situation has several inherent limitations, mainly owing to assumptions with regard to geometry, contact, loading and region of interest. This study has neglected the gingiva soft tissue and inferior mandibular canal in the modelling. Besides, the bone-implant attachment was assumed to be perfectly bonded to demonstrate a complete osseointegration although histological studies reported the level of osseointegration varied from 30–70%. For the loading, it was applied at one localised point only on the prosthesis surface opposed to multiple points on the cusp during actual occlusion. Also, the findings from this work shed light on the restoration of the mandibular first molar tooth, suggesting that the results can only be applied to this set of teeth. Different outcomes might be obtained in the maxillary model that having a lower bone quality and quantity. Several aspects can be improved in future studies, such as considering more complex geometry, varying dimensions and macro-geometries of the implant and applying reversal implant removal from the bone. Despite the robust findings of this computational study, it was necessary to perform *in vitro* and *in vivo* clinical studies to validate the mechanical stimuli transfer and prognosis of the implant even at the basic level.

5. Conclusions

Within the limitations of this study, the following conclusions can be drawn. It is demonstrated that the implant stiffness is the most effective factor in increasing mechanical stimuli transfer to the bone when both stress and strain energy density are concerned. The interaction between the implant stiffness and horizontal load magnitude is found to be significant and effective in decreasing the likelihood of bone loss.

Reducing the implant stiffness and horizontal load value leads to the increased stress transfer to the bone, however, the strain energy density is decreased, except for the case with low horizontal load value. The increase in the implant stiffness and horizontal load value (up to medium level) have increased the strain energy transfer to the bone. The role of both factors is vital and should be addressed in the pre-operative treatment planning and design of dental implant.

Acknowledgements

References

[1] ARMENTIA M., ABASOLO M., CORIA I., ALBIZURI J., *Fatigue design of dental implant assemblies: a nominal stress approach*, Metals, 2020, 10 (6), DOI: 10.3390/met10060744.

[2] BATAINEH K., AL JANAIDEH M., *Effect of different biocompatible implant materials on the mechanical stability of dental implants under excessive oblique load*, Clin. Implant. Dent. Relat. Res., 2019, 21 (6), DOI: 10.1111/cid.12858.

[3] BAYATA F., YILDIZ C., *The effects of design parameters on mechanical failure of Ti-6Al-4V implants using finite element analysis*, Eng. Fail. Anal., 2020, 110, DOI: 10.1016/j.engfailanal.2020.104445.

[4] BIDEZ M.W., MISCH C.E., Chapter 5 – *Clinical Biomechanics in Implant Dentistry*, Mosby, 2015.

[5] DANTAS T.A., CARNEIRO NETO J.P., ALVES J.L., VAZ P.C.S., SILVA F.S., *In silico evaluation of the stress fields on the cortical bone surrounding dental implants: comparing root-analogue and screwed implants*, J. Mech. Behav. Biomed. Mater, 2020, 104, DOI: 10.1016/j.jmbbm.2020.103667.

[6] ELIAS D.M., VALERIO C.S., DE OLIVEIRA D.D., MANZI F.R., ZENÓBIO E.G., SERAIDARIAN P.I., *Evaluation of different heights of prosthetic crowns supported by an ultra-short implant using three-dimensional finite element analysis*, Int. J. Prosthodont., 2020, 33 (1), DOI: 10.11607/ijp.6247.

[7] FIORELLINI J.P., SOURVANOS D., SARIMENTO H., KARIMBUX N., LUAN K.W., *Periodontal and implant radiology*, Dent. Clin. N. Am., 2021, 65 (3), DOI: 10.1016/j.cden.2021.02.003.

[8] GEFEN A., *Optimizing the biomechanical compatibility of orthopedic screws for bone fracture fixation*, Med. Eng. Phys., 2002, 24 (5), DOI: 10.1016/S1350-4533(02)00027-9.

[9] HAASE K., ROUHI G., *Prediction of stress shielding around an orthopedic screw: using stress and strain energy density as mechanical stimuli*, Comput. Biol. Med., 2013, 43 (11), DOI: 10.1016/j.compbiomed.2013.07.032.

[10] IBRAHIM M.I.F., ROSLI M.U., ISHAK M.I., ZAKARIA M.S., JAMALLUDIN M.R., KHOR C.Y., RAHIM W.M.F.W.A., NAWI M.A.M., SHAHRIN S., *Simulation-based optimization of injection molding parameter for meso-scale product of dental component fabrication using response surface methodology*

(RSM), AIP Conf. Proc., 2018, 2030 (1), DOI: 10.1063/1.5066719.

[11] Iᴀʜᴀᴋ M.I., Aʙᴅᴜʟ Kᴀᴅɪʀ M.R., *Biomechanics in Dentistry: Evaluation of Different Surgical Approaches to Treat Atrophic Maxilla Patients*, Springer, 2013.

[12] Iᴀʜᴀᴋ M.I., Dᴀᴜᴅ R., Iʙʀᴀʜɪᴍ I., Mᴀᴛ F., Mᴀɴꜱᴏʀ N.N., *A review of factors influencing peri-implant bone loss*, AIP Conf. Proc., 2021, 2347 (1), DOI: 10.1063/5.0051600.

[13] Iᴀʜᴀᴋ M.I., Sʜᴀғɪ A.A., Rᴏꜱʟɪ M.U., Kʜᴏʀ C.Y., Zᴀᴋᴀʀɪᴀ M.S., Rᴀʜɪᴍ W.M.F.W.A., Jᴀᴍᴀʟʟᴜᴅɪɴ M.R., *Biomechanical evaluation of different abutment-implant connections – a nonlinear finite element analysis*, AIP Conf. Proc., 2017, 1885 (1), DOI: 10.1063/1.5002258.

[14] Kʜᴏʀ C.Y., Iᴀʜᴀᴋ M.I., Rᴏꜱʟɪ M.U., Jᴀᴍᴀʟʟᴜᴅɪɴ M.R., Zᴀᴋᴀʀɪᴀ M.S., Yᴀᴍɪɴ A.F.M., Aʙᴅᴜʟ Aᴢɪᴢ M.S., Aʙᴅᴜʟʟᴀʜ M.Z., *Influence of material properties on the fluid-structure interaction aspects during molded underfill process*, MATEC Web. Conf., 2017, 97, DOI: 10.1051/matecconf/20179701059.

[15] Kɪᴍ W.H., Lᴇᴇ J.-C., Lɪᴍ D., Hᴇᴏ Y.-K., Sᴏɴɢ E.-S., Lɪᴍ Y.-J., Kɪᴍ B., *Optimized dental implant fixture design for the desirable stress distribution in the surrounding bone region: a biomechanical analysis*, Materials, 2019, 12 (17), DOI: 10.3390/ma12172749.

[16] Lɪᴜ C., Xɪɴɢ Y., Lɪ Y., Lɪɴ Y., Xᴜ J., Wᴜ D., *Bone quality effect on short implants in the edentulous mandible: a finite element study*, BMC Oral Health, 2022, 22 (1), DOI: 10.1186/s12903-022-02164-8.

[17] Mᴀᴄᴇᴅᴏ J.P., Pᴇʀᴇɪʀᴀ J., Fᴀʀɪᴀ J., Sᴏᴜᴢᴀ J.C.M., Aʟᴠᴇꜱ J.L., Lóᴘᴇᴢ-Lóᴘᴇᴢ J., HᴇɴʀɪQᴜᴇꜱ B., *Finite element analysis of peri-implant bone volume affected by stresses around Morse taper implants: effects of implant positioning to the bone crest*, Comput. Methods Biomech. Biomed. Engin., 2018, 21 (12), DOI: 10.1080/10255842.2018.1507025.

[18] Mᴀɴɢᴀɴᴏ F.G., Sʜɪʙʟɪ J.A., Sᴀᴍᴍᴏɴꜱ R.L., Iᴀᴄᴜʟʟɪ F., Pɪᴀᴛᴛᴇʟʟɪ A., Mᴀɴɢᴀɴᴏ C., *Short (8-mm) locking-taper implants supporting single crowns in posterior region: a prospective clinical study with 1-to 10-years of follow-up*, Clin. Oral Implants Res., 2014, 25 (8), DOI: 10.1111/clr.12181.

[19] MᴀQᴜᴇᴛ P., Wᴏʟғғ J., Fᴜʀʟᴏɴɢ R., *The Law of Bone Remodelling*, Springer, Berlin Heidelberg, 2012.

[20] Mᴀʀᴄɪáɴ P., Wᴏʟғғ J., Hᴏʀáᴄ̌ᴋᴏᴠá L., Kᴀɪꜱᴇʀ J., Zɪᴋᴍᴜɴᴅ T., Bᴏʀáᴋ L., *Micro finite element analysis of dental implants under different loading conditions*, Comput. Biol. Med., 2018, 96, DOI: 10.1016/j.compbiomed.2018.03.012.

[21] Nᴀᴊᴇᴇʙ S., Mᴀʟɪ M., YᴀQɪɴ S.A.U., Zᴀғᴀʀ M.S., Kʜᴜʀꜱʜɪᴅ Z., Aʟᴡᴀᴅᴀᴀɴɪ A., Mᴀᴛɪɴʟɪɴɴᴀ J.P., Chapter 21: *Dental Implants Materials and Surface Treatments*, Woodhead Publishing, 2019.

[22] Nᴀᴠᴇᴀᴜ A., Sʜɪɴᴍʏᴏᴜᴢᴜ K., Mᴏᴏʀᴇ C., Aᴠɪᴠɪ-Aʀʙᴇʀ L., Jᴏᴋᴇʀꜱᴛ J., Kᴏᴋᴀ S., *Etiology and measurement of peri-implant crestal bone loss (CBL)*, J. Clin. Med., 2019, 8 (2), DOI: 10.3390/jcm8020166.

[23] Nᴀᴡɪ M.A.M., Rᴀᴢᴍᴀɴ Aᴍɪɴ M., Kᴀꜱɪᴍ M.S., Iᴢᴀᴍꜱʜᴀʜ R., Iᴀʜᴀᴋ M.I., Kʜᴏʀ C.Y., Rᴏꜱʟɪ M.U., Jᴀᴍᴀʟʟᴜᴅɪɴ M.R., Mᴏʜᴀᴍᴀᴅ SʏᴀғɪQ A.K., *The influence of spiral blade distributor on pressure drop in a swirling fluidized bed*, IOP Conf Ser: Mater. Sci. Eng., 2019, 551 (1), DOI: 10.1088/1757-899x/551/1/012106.

[24] Nɪʀᴏᴏᴍᴀɴᴅ M.R., Aʀᴀʙʙᴇɪᴋɪ M., *Implant stability in different implantation stages: analysis of various interface conditions*, Inform. Med. Unlocked, 2020, 19, DOI: 10.1016/j.imu.2020.100317.

[25] Oᴅɪɴ G., Sᴀᴠᴏʟᴅᴇʟʟɪ C., Bᴏᴜᴄʜᴀʀᴅ P.-O., Tɪʟʟɪᴇʀ Y., *Determination of Young's modulus of mandibular bone using inverse analysis*, Med. Eng. Phys., 2010, 32 (6), DOI: 10.1016/j.medengphy.2010.03.009.

[26] Oᴍᴀʀ A., Iᴀʜᴀᴋ M.I., Hᴀʀᴜɴ M.N., Sᴜʟᴀɪᴍᴀɴ E., Kᴀꜱɪᴍ N.H.A., *Effects of different angulation placement of mini-implant in orthodontic*, Appl. Mech. Mater., 2012, 121–126, DOI: 10.4028/www.scientific.net/AMM.121-126.1214.

[27] Pᴀᴛɪʟ S.M., Dᴇꜱʜᴘᴀɴᴅᴇ A.S., Bʜᴀʟᴇʀᴀᴏ R.R., Mᴇᴛᴋᴀʀɪ S.B., Pᴀᴛɪʟ P.M., *A three-dimensional finite element analysis of the influence of varying implant crest module designs on the stress distribution to the bone*, Dent. Res. J. (Isfahan), 2019, 16 (3), 145–152.

[28] Pᴇʀʀᴇɴ S.M., Hᴜɢɢʟᴇʀ A., Rᴜꜱꜱᴇɴʙᴇʀɢᴇʀ M., Aʟʟɢöᴡᴇʀ M., Mᴀᴛʜʏꜱ R., Sᴄʜᴇɴᴋ R., Wɪʟʟᴇɴᴇɢɢᴇʀ H., Müʟʟᴇʀ M.E., *The reaction of cortical bone to compression*, Acta Orthop. Scand. Suppl., 1969, 125.

[29] Pʀᴏᴄʜᴏʀ P., Fʀᴏꜱꜱᴀʀᴅ L., Sᴀᴊᴇᴡɪᴄᴢ E., *Effect of the material's stiffness on stress-shielding in osseointegrated implants for bone-anchored prostheses: a numerical analysis and initial benchmark data*, Acta Bioeng. Biomech., 2020, 22 (2), DOI: 10.37190/ABB-01543-2020-02.

[30] Qɪɴ W., Cᴏɴɢ M., Rᴇɴ X., Wᴇɴ H., *Design of realistic chewing trajectory for dynamic analysis of the dental prosthesis*, Acta Bioeng. Biomech., 2020, 22 (3), DOI: 10.37190/ABB-01581-2020-02.

[31] Rᴏʙᴀᴜ-Pᴏʀʀᴜᴀ A., Péʀᴇᴢ-Rᴏᴅʀíɢᴜᴇᴢ Y., Sᴏʀɪꜱ-Rᴏᴅʀíɢᴜᴇᴢ L.M., Péʀᴇᴢ-Aᴄᴏꜱᴛᴀ O., Gᴏɴᴢáʟᴇᴢ J.E., *The effect of diameter, length and elastic modulus of a dental implant on stress and strain levels in peri-implant bone: a 3D finite element analysis*, Biomed. Mater Eng., 2020, 30, DOI: 10.3233/BME-191073.

[32] Sᴄʜᴡɪᴛᴀʟʟᴀ A.D., Aʙᴏᴜ-Eᴍᴀʀᴀ M., Sᴘɪɴᴛɪɢ T., Lᴀᴄᴋᴍᴀɴɴ J., Müʟʟᴇʀ W.D., *Finite element analysis of the biomechanical effects of PEEK dental implants on the peri-implant bone*, J. Biomech., 2015, 48 (1), DOI: 10.1016/j.jbiomech.2014.11.017.

[33] Sʜᴇᴍᴛᴏᴠ-Yᴏɴᴀ K., Rɪᴛᴛᴇʟ D., *On the mechanical integrity of retrieved dental implants*, J. Mech. Behav. Biomed. Mater, 2015, 49, DOI: 10.1016/j.jmbbm.2015.05.014.

[34] Sᴏᴍᴍᴇʀ M., Zɪᴍᴍᴇʀᴍᴀɴ J., Gʀɪᴢᴇ L., Sᴛüʙɪɴɢᴇʀ S., *Marginal bone loss one year after implantation: a systematic review of different loading protocols*, Int. J. Oral Maxillofac. Surg., 2020, 49 (1), DOI: 10.1016/j.ijom.2019.03.965.

[35] Sᴛᴀɴғᴏʀᴅ C.M., Bʀᴀɴᴅ R.A., *Toward an understanding of implant occlusion and strain adaptive bone modeling and remodeling*, J. Prosthet. Dent., 1999, 81 (5), DOI: 10.1016/S0022-3913(99)70209-X.

[36] Tᴇᴋɪɴ S., Dᴇğᴇʀ Y., Dᴇᴍɪʀᴄɪ F., *Evaluation of the use of PEEK material in implant-supported fixed restorations by finite element analysis*, Niger J. Clin. Pract., 2019, 22 (9), DOI: 10.4103/njcp.njcp_144_19.

[37] Tʀɪʙꜱᴛ J.P.M., Dᴀʟ Pɪᴠᴀ A.M.D.O., Bᴏʀɢᴇꜱ A.L.S., Bᴏᴛᴛɪɴᴏ M.A., *Influence of socket-shield technique on the biomechanical response of dental implant: three-dimensional finite element analysis*, Comput. Methods Biomech. Biomed. Engin., 2020, 23 (6), DOI: 10.1080/10255842.2019.1710833.

[38] Tᴜʀɴᴇʀ C.H., *Three rules for bone adaptation to mechanical stimuli*, Bone, 1998, 23 (5), DOI: 10.1016/S8756-3282(98)00118-5.

[39] Vᴀʜᴅᴀᴛɪ A., Rᴏᴜʜɪ G., *A model for mechanical adaptation of trabecular bone incorporating cellular accommodation and effects of microdamage and disuse*, Mech. Res. Commun., 2009, 36 (3), DOI: 10.1016/j.mechrescom.2008.10.004.

[40] WĄDOŁOWSKI P., KRZESIŃSKI G., GUTOWSKI P., *Finite element analysis of mini-plate stabilization of human mandible angle fracture – a comparative study*, Acta Bioeng. Biomech., 2020, 22 (3), DOI: 10.37190/ABB-01617-2020-02.

[41] YALÇIN M., KAYA B., LAÇIN N., ARI E., *Three-dimensional finite element analysis of the effect of endosteal implants with different macro designs on stress distribution in different bone qualities*, Int. J. Oral Maxillofac. Implants, 2019, 34 (3), DOI: 10.11607/jomi.7058.